IOSR Journal of Engineering (IOSRJEN) **www.iosrjen.org**
ISSN (e): 2250-3021, ISSN (p): 2278-8719
Vol. 06, Issue 07 (July. 2016), ||V2|| PP 57-67

Reconstructing ISAR Target via Dipole Model

Dr. Ali Nassib[1], Yasar Guzel[2]
[1]*University of Dayton*
nassib123@gmail.com
[2]*University of Dayton*
nasarguzel.yg@gmail.com

Abstract: **-** This paper addresses a unique method of ISAR dipole model image by employing vector dyadic contrast function technique. The current ISAR imaging algorithms rely upon the assumption that the area under investigation consists of a superposition of infinitesimally small isotropic scatterers (i.e., the point scatterer model). This approximation fails to capture the true real-world scattering mechanisms occurring within the targets of interest. Therefore, this paper proposes a batter imaging technique which based upon the assumption that targets can be modeled as a collection of infinitesimally small dipoles. The orientation of each dipole is accounted in a dyadic contrast function. The image reconstruction, i.e., retrieval of the dyadic reflectivity function from measured data, will not only provide information regarding the shape but also the direction of predominant edges of the target.

Keywords: **-** *Inverse synthetic aperture radar (ISAR); Dipole model (DM), Point scatterer model.*

I. INTRODUCTION

The inverse scattering problem is a one that determines the nature of a target of interest from the knowledge of the scattered electromagnetic fields. Figure 1 shows two cylinders oriented vertically and illuminated with a monochromatic plane wave, after the interaction of the incident plane wave with the target, the scattered fields are measured by recievers placed in the near field of the target. The methods used for solving inverse problems depend upon the electrical size of the target in a medium. If D is the characteristic dimension of the scatterer and k is the wavenumber, the quantity k*D gives a measure of the electrical length of the target. When k*D << 1, scattering is weak, and we may apply low frequency methods as well as the Rayleigh and Born approximations. On the other hand, when k*D >>1, we may use high frequency asymptotic techniques such as geometrical or physical optics methods [1], [2]. The main contribution of this research is enhanced imaging of targets under observation using a novel sensing approach in which the orientation of the current dipole is a critical variable for interference suppression and feature exploitation. Using vector dyadic reflectivity function, small features are better observed, even when in the presence of dominant scatterers.

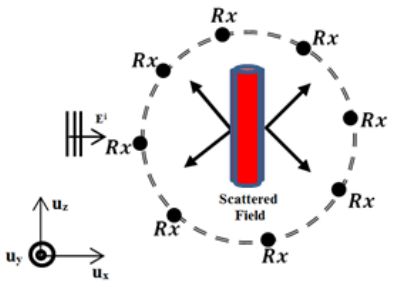

Fig.1. Inverse Scattering Problem.

II. INVERSE SYNTHETIC APERTURE RADAR (ISAR)

(ISAR) provides a powerful sensing and signal processing technique for imaging moving targets in the range and cross-range domains, as shown in (Figure 2). This technique is developed based upon the fundamental assumption that the target to be imaged is a collection of infinitesimally small isotropic sources. In ISAR, cross-range resolution is limited by the extent of the platform (or target) motion, e.g., translation and rotation within the antenna main beam over an observation interval. Extended dwell time processing allows for improved resolution [3]. However, as the target rotates (and translates), the scattered electric fields changes both in phase and amplitude, invalidating the fundamental assumption of isotropic point target scattering. As target returns decorrelate over time and observation angle, a coherently-formed ISAR image will degrade. Typically, this problem is mitigated by reducing the coherent dwell to a value that will "likely" preserve the target's exploitable electromagnetic signature.

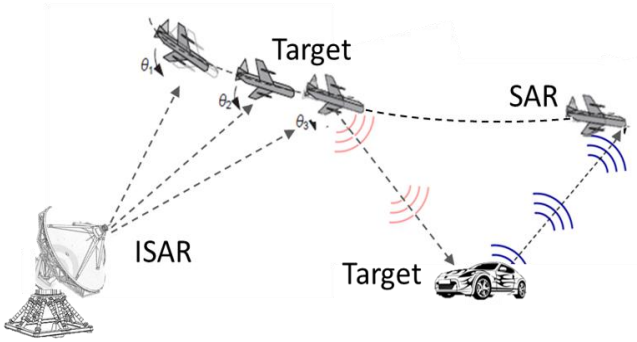

Fig. 2. ISAR and SAR imaging of rotating targets.

Many researchers have addressed the problem of wide angle ISAR imaging, with very successful results. Some approaches resort to computationally-intense signal processing to correct for phase errors. Other approaches simply compute a set of coherently-formed images, and then attempt to "merge" such images to form an improved representation of the target. These methods are all useful, but a substantial increase in performance could be achieved if the underlying model captured more realistically the scattering phenomena and mechanisms occurring at the target. From a pure electromagnetic perspective, the scattering process occurring at a target is properly described using the electric field integral equation (EFIE) and the magnetic field integral equation (MFIE). In principle, if ISAR data is processed using the EFIE and MFIE as the scattering model, then the entire data set could be processed coherently, leading to an extremely accurate representation of the target [1], [2], [4].

$$\overbrace{\mathbf{E}(\mathbf{r}) = -\frac{i\omega\mu}{4\pi}\int_V \left[\left[\bar{\mathbf{I}} + \frac{\nabla\nabla}{k^2}\right] G_0(\mathbf{r},\mathbf{r}')\right]\cdot \mathbf{J}(\mathbf{r}')\, d\mathbf{r}'}^{EFIE\ in\ the\ form\ of\ dyadic} \quad (1)$$

$$\overbrace{\mathbf{H}(\mathbf{r}) = -\frac{1}{i\omega\mu}\nabla\times\mathbf{E}(\mathbf{r})}^{MFIE\ in\ the\ form\ of\ dyadic} \quad (2)$$

Practically, inversion of the EFIE of equation (1) or MFIE equation (2) is extremely difficult because when electromagnetic fields scatter from thin wires, we must solve an integral equation of first kind, with complex kernels. These integrals are inherently non-linear and ill-posed, meaning that the solutions are generally unstable and small physical changes may cause very large changes in the results, plus they are computationally intensive. Therefore, we propose a scattering model that lies in between the rigorous EFIE/MFIE interpretation and the point-scattering assumption [5]. Specifically:

1) The target consists of a collection of infinitesimally small dipoles with arbitrary orientation,
2) The target's internal multipath is negligible, meaning the first order Born approximation holds, and the linearized equation as shown below is applicable.

$$\mathbf{E}^{tot}(r) = \mathbf{E}^{i}(r) + k_0^2 \int_V \mathrm{G}_0(\mathrm{r},\mathrm{r}') \cdot \mathbf{E}^{tot}(r)\, \boldsymbol{\rho}(r')\, dr' \qquad (3)$$

$$= \mathbf{E}^{i}(r) + \mathbf{E}^{s}(r)$$

In this equation, $\mathbf{E}^{s}(r,r')$ is the scattered field resulting from the interaction of the incident wave $\mathbf{E}^{i}(r,r')$ with the contrast function $\boldsymbol{\rho}(r')$, and $\mathbf{G}_0(r,r')$ is the free space Green's function. Using the far field approximation for the radiated spherical wave $\mathbf{G}_0(r,r')$ we obtain

$$\mathbf{E}^{s}(r,r') = k_0^2 \int_V \mathbf{G}_0(r,r')(r,r') \cdot \mathbf{E}^{i}(r,r')\, \boldsymbol{\rho}(\mathbf{r}')\, dr' \qquad (4)$$

When adopting the first order Born approximation, the total field $\mathbf{E}^{tot}(r,r')$ in equation (4) is replaced with the incident field $\mathbf{E}^{i}(r,r')$ which leads to linear equation. The Born approximation is based upon weak scattering phenomena which occur when the incident wave is only scattered once and this incident wave basically undergoes very little perturbation as it interacts with the target of interest. This is beneficial in that the wave can generally be approximated as the incident field, allowing the problem to be linearized in order to find a solution. By linearizing the problem one can establish a Fourier relationship between the measured scattered field data and the object/contrast function [5], [6].

The problem of determining the image of an object from scattered fields has received a great deal of attentions due to the myriad of applications. For objects that are sufficiently weakly scattering, its well-known that the inverse scattering problem can be linearized as equation (3) shows and image reconstruction can be achieved by extracting the Fourier data describing the target from scattered fields. In other words, the success of this approximation is dependent upon the target being modeled as a collection of weak scatterers. The target is assumed to be a wire-frame representation of the original, and the goal is to reconstruct an image of the target of interest. At this stage, small metallic surfaces are often represented by their thin-wire boundary approximation. Inclusion of a patch model would dramatically complicate the mathematical formulation. Irregular metallic patches may reflect the energy diffusely in a variety of different directions, thus providing a small contribution to the reflected energy. If the receiver's direction is pointing near the specular region of the metallic patch under illumination, then the resulting scattering process can be equally described as a superposition of many infinitesimally small dipoles oriented along the same polarization as the incident waveform and distributed along the entire surface of the metallic patch. In essence, the scattering processes due to flat metallic patches are accounted for in the dipole model. The idea of extending the point-scattering model to a dipole model is not new. Several researchers, especially B. Yazici and M. Gustaffson [7], have realized the importance of such developments and have proposed imaging schemes based upon exploitation of a dipole model of a target.

What we explore in this paper is the incorporation a targets' dipole locations *and* direction under a simple 3x3 matrix function (i.e., a dyadic function). This can be estimated using classical back-projection algorithms. In other words, extending the scattering model from a point target to a dipole target would only require invoking the existing ISAR algorithms multiple (3 by 3 matrix) times.

As shown in the result (section 5) below, the reconstructed "dyadic" image (which can either be interpreted as nine different but interrelated images, or a single image with each pixel having 9 parameters) is unintelligible, but the structure of each 3x3 dyadic "pixel" incorporates the direction of the dipole scatterer included within. Another important advantage obtained using a dipole model is the capability to provide additional information about each reconstructed pixel - information that can be used for better target recognition. Many researchers have developed feature extraction algorithms that attempt to retrieve shapes including plates, corner reflectors, edges, cylinders, conical sections, or spheres, from the target's scattered waveform [8]. This additional information provides extra dimensions in the feature space for better classification and identification. A dipole-based representation of the target will provide additional dimensions to the feature space. The next sections describe a mathematical formulation of the forward and inverse problem, as well as simulations and forthcoming experiments [9], [10].

III. IMAGING WITH A DIPOLE MODEL

The proposed model assumes that the target consists of a collection of dipole scatterers (see Figure 3). Up to now we have only discussed the inverse scattering infinitesimal dipole model, where the target is located in a homogeneous background medium [5], [6].

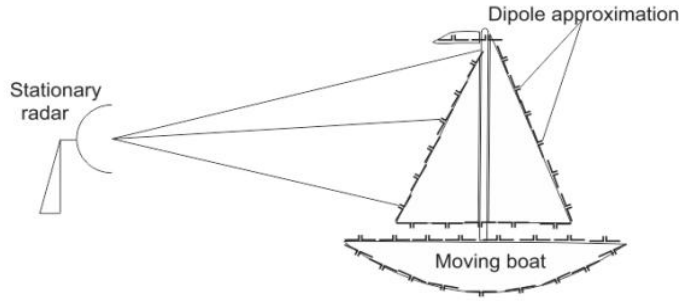

Fig. 3. Target model is based upon a vector summation of small dipoles.

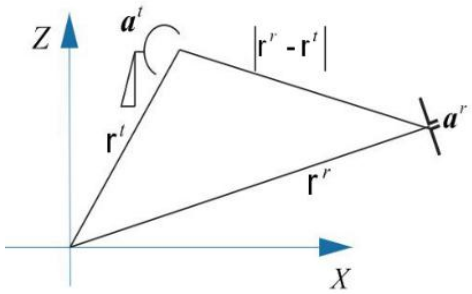

Fig. 4. Source and small dipole model.

Consider a transmitter located at $\mathbf{r}^t$ emitting a waveform polarized along the vector $\mathbf{a}^t$, a receiver located at $\mathbf{r}^r$ polarized along the vector $\mathbf{a}^r$, and a point under illumination at location $\mathbf{r}$. The time-harmonic incident electric field at location **r** is shown below.

$$\boldsymbol{E}^{i} = \bar{\mathbf{G}} \cdot \mathbf{a}^{t}$$

$$= \begin{bmatrix} E_x^i \\ E_y^i \\ E_z^i \end{bmatrix} = \begin{bmatrix} a_x^t G_{xx} + & a_y^t G_{xy} + & a_z^t G_{xz} \\ a_x^t G_{yx} + & a_y^t G_{yy} + & a_z^t G_{yz} \\ a_x^t G_{zx} + & a_y^t G_{zy} + & a_z^t G_{zz} \end{bmatrix} \qquad (5)$$

where, $\bar{\mathbf{G}}$ is the free space far fields dydic Green's function of the background medium which relates the vector electromagnetic fields to vector current source. Using the principle of linear superposition, the solution of the field due to a general source is the convolution of the green's function with the source [4], [11].

Let us assume that an infinitesimally small dipole oriented along **t** is present at point **r**. When the electric field **e** impinging on **r** is parallel to **t,** then a current **j** is induced on the dipole. This current will generate a scattered field propagating in all directions, and towards the receiver antenna. The measured electric field will be.

$$\boldsymbol{E}^{s} = \mathbf{a}^{r} \cdot \bar{\mathbf{G}} \cdot \mathbf{J} \tag{6}$$

$$= \begin{bmatrix} E_x^s \\ E_y^s \\ E_z^s \end{bmatrix} = \begin{bmatrix} a_x^r G_{xx} + & a_y^r G_{yx} + & a_z^r G_{zx} \\ a_x^r G_{xy} + & a_y^r G_{yy} + & a_z^r G_{zy} \\ a_x^r G_{xz} + & a_y^r G_{yz} + & a_z^r G_{zz} \end{bmatrix}^T \cdot \begin{bmatrix} J_x \\ J_y \\ J_z \end{bmatrix}$$

Clearly, if the small dipole is not oriented along the incident field, only a fraction of the current is excited. Mathematically, the current induced in the dipole **t** can be expressed as [12], [13], [14].

$$\mathbf{j}(\mathbf{r}) = \frac{\left[\boldsymbol{E}^{i}(\mathbf{r}) \cdot \mathbf{t}(\mathbf{r})\right]\mathbf{t}(\mathbf{r})}{\left\|\mathbf{t}(\mathbf{r})\right\|} \tag{7}$$

After some mathematical manipulation, equation (7) can be rewritten in dyadic form as shown below.

$$\mathbf{j}(\mathbf{r}) = \begin{bmatrix} t_x^2(\mathbf{r}) & t_x(\mathbf{r})t_y(\mathbf{r}) & t_x(\mathbf{r})t_z(\mathbf{r}) \\ t_x(\mathbf{r})t_y(\mathbf{r}) & t_y^2(\mathbf{r}) & t_y(\mathbf{r})t_z(\mathbf{r}) \\ t_z(\mathbf{r})t_x(\mathbf{r}) & t_z(\mathbf{r})t_y(\mathbf{r}) & t_z^2(\mathbf{r}) \end{bmatrix} \cdot \frac{\boldsymbol{E}^{i}(\mathbf{r})}{\left\|\mathbf{t}(\mathbf{r})\right\|} \tag{8}$$

$$= \frac{1}{\left\|\mathbf{t}(\mathbf{r})\right\|}\boldsymbol{\rho}(\mathbf{r}) \cdot \boldsymbol{E}^{i}(\mathbf{r})$$

where, $\mathbf{a}^{r}$ the polarization vector of is scattered electric field and $\mathbf{a}^{t}$ is the polarization vector of the incident wave. Now let us assume that the receiving antenna has a particular polarization such that it collects the scattered field in the $\mathbf{a}^{r}$ direction [5], [15], [16]. Equation (6) is modified as shown below:

$$\overbrace{\boldsymbol{E}^{s}(\boldsymbol{r})}^{Scattered\ electric\ field} = \int_{s} \left(\mathbf{a}^{r}\right)^{T} \cdot \bar{\mathbf{G}}\left(\mathbf{r}^{r}, \mathbf{r}\right) \cdot \boldsymbol{\rho}\left(\mathbf{r}'\right) \cdot \mathbf{G}\left(\mathbf{r}, \mathbf{r}^{t}\right) \cdot \mathbf{a}^{t} \cdot d\mathbf{r} \tag{9}$$

where, $\boldsymbol{\rho}(\mathbf{r})$ is the contrast function and has the same meaning as the classical reflectivity function in ISAR, with the difference that for each point **r** there exists nine different parameters to be estimated [3], [17].

Using the dyadic notation, equation (9) is transformed into a discrete form as:

$$\boldsymbol{E}^{s} = \sum_{n=1}^{P} \left(\mathbf{a}^{r}\right)^{T} \cdot \bar{\mathbf{G}}\left(\mathbf{r}^{r}, \mathbf{r}_n\right) \cdot \rho\left(\mathbf{r}_n\right) \cdot \bar{\mathbf{G}}\left(\mathbf{r}_n, \mathbf{r}^{t}\right) \cdot \mathbf{a}^{t} \tag{10}$$

Where, *D* is the domain of interest $\mathbf{r}_n$ is the location of the *n*th pixel, *P* is the total number of pixels, and $\rho\left(\mathbf{r}_n\right)$ is the unknown reflectivity/contrast function which looks like as follows [9], [5].

$$\overbrace{\rho(\mathbf{r}_n)}^{Reflectivity\ function\ in\ dyadic\ form} = \begin{bmatrix} \rho_{xx} & \rho_{xy} & \rho_{xz} \\ \rho_{yx} & \rho_{yy} & \rho_{yz} \\ \rho_{zx} & \rho_{zy} & \rho_{zz} \end{bmatrix} \tag{11}$$

where, the contrast function $\rho(\mathbf{r}_n)$ is composed of the sum of the main diagonal and off-diagonal elements. The first term which is the main diagonal matrix represents the effects of the target when there is no depolarization. While the off-diagonal is non zero when there is a depolarization. The second term is obtained through dyadic product.

IV. FORMATION OF A MATRIX EQUATION

Mathematically, the problem of finding the reflectivity function requires that we compute the inverse linear operator of equation (10) . This is the dipole-based forward scattering model, and relates the unknown reflectivity dyadic function $\rho(\mathbf{r}_n)$ to the measured signal. However, equation (10) returns the value corresponding to a single measurement, i.e., a specific transmitter location and orientation, a specific receiver location and orientation, and a specific frequency. If any of these parameters vary, a new measurement must be acquired. Let us collect a set of (m = 1, M) measurements. For a specific measurement m and a specific pixel p, equation (10) can be rewritten as shown below [5], [9]:

$$\begin{aligned} \boldsymbol{E}_{mp} &= l_{mp}^{xx}\rho_{mp}^{xx} + l_{mp}^{xy}\rho_{mp}^{xy} + l_{mp}^{xz}\rho_{mp}^{xz} + \dots \\ &\quad + l_{mp}^{yx}\rho_{mp}^{yx} + l_{mp}^{yy}\rho_{mp}^{yy} + l_{mp}^{yz}\rho_{mp}^{yz} + \dots \\ &\quad + l_{mp}^{zx}\rho_{mp}^{zx} + l_{mp}^{zy}\rho_{mp}^{zy} + l_{mp}^{zz}\rho_{mp}^{zz} \\ &= \mathbf{l}_{mp}^{T} \cdot \boldsymbol{\rho}_{mp} \end{aligned} \tag{12}$$

where, each value of $\boldsymbol{l}$ can be determined by properly re-arranging and recasting the terms in of the result in (10) . By extending the above equation to all pixels in the region D and all possible measurement configurations M, one obtains:

$$\underbrace{\begin{bmatrix} e_1 \\ \vdots \\ e_M \end{bmatrix}}_{\mathbf{e}^s} = \underbrace{\begin{bmatrix} \mathbf{l}_{11}^T & \cdots & \mathbf{l}_{1P}^T \\ \vdots & \ddots & \vdots \\ \mathbf{l}_{M1}^T & \cdots & \mathbf{l}_{MP}^T \end{bmatrix}}_{\mathbf{L}} \underbrace{\begin{bmatrix} \boldsymbol{\rho}_{11} \\ \vdots \\ \boldsymbol{\rho}_{MP} \end{bmatrix}}_{\rho} \tag{13}$$

$$\overbrace{\mathbf{E}^s}^{Scattered/Measured} = \overbrace{\mathbf{L}}^{Geometry} \cdot \overbrace{\boldsymbol{\rho}}^{Image\ function}$$

Simply speaking, $\mathbf{E}^s$ is a (known) vector containing all measurements collected at different positions / directions / frequencies, $\mathbf{L}$ is a (large) matrix whose entries can be calculated theoretically from equation (10),

and $\boldsymbol{\rho}(\mathbf{r})$ is a vector representing the (dyadic) reflectivity function of the target. After the creation of the **L** matrix from equation (10), equation(13) known as forward model must be inverted in order to recover the dyadic reflectivity function. The easiest way to invert equation (13) is to employ any regularized method either direct such as Truncated Singular Value Decomposition (TSVD) or iterative method such as Conjugate Gradient (CGM). This paper conjugate gradient method is used for inversion [5], [18].

CGM is the most prominent iterative mothed for solving linear equation. Iterative methods of solving $\mathbf{E}^s = \mathbf{L} \cdot \boldsymbol{\rho}$, such as the conjugate gradient method, create a sequence of approximations that converge in theory to the exact solution [19], [20]. These methods require forming products $\mathbf{L} \cdot \boldsymbol{\rho}$ and updating $\mathbf{E}^s$ as a result.

V. SIMULATION RESULTS

The proposed algorithm was tested using an accurate EM simulation software tool known as FEKO and Matlab to reconstruct a 2D image of two thin cylinders with three different orientations. In this example we have done three cases. In the first case we both placed two thin cylinders and source along x-direction. The second case we placed the two thin cylinders and again source along y-direction. The third case we placed two cylinders along x-direction with source and another two cylinders along y-direction with another separate source which forms a ring comprising four cylinders shaped as a square.

In this 2D simulations, the transmitting and receiving antennas are located in the x-y plane. In the simulation we used 72 transmitters and 72 receivers. All 144 antennas are assumed to transmit and receive either one of the three orthogonal polarizations $(\hat{\mathbf{x}}, \hat{\mathbf{y}}\ and\ \hat{\mathbf{z}})$. The transmitting antennas are placed along a radius of 13λ and the receiving antennas are also placed at 10λ with respect to the target. The operating frequency is 10 GHz $(\lambda = 3cm)$ and the total measurement collected size is $(N_t \times N_r \times 9 = 72 * 72 * 9 = 46656)$; where N_t and N_r are number of transmitters and receivers and the 9 values of reflectivity function. The area under investigation is 0.4 m by 0.4 m, which divided into pixels with a size of 0.05λ and comprised of $(N_t \times N_r \times 9 = 72 * 72 * 9 = 46656\ unknowns)$. Data is collected using a sensor platform encircling the target of interest (TI). After the scattered field is collected, we computed the **L** matrix from equation (10) as stated earlier in (section 3-4). **L** matrix is nothing more than computing the dyadic Green's function in homogeneous medium through Matlab. In equation (10) the dyadic Green's function relates the transmitter to the target of interest (TI) and from the target back to the receiver. After acquiring $\mathbf{E}^s$ through FEKO simulation and calculated the L matrix, we generated the image of the target by employing technique known as conjugate gradient method (CGM).

The objective of this simulation is to employ the vector dyadic reflectivity function which comprises nine elements rather than one scalar element. The nine elements not only allow us to determine: 1) the location, but also 2) the orientation of the electrically small dipole in which the scalar con not be determined due to the point source model. (Figures 6, 8, and 10) are base on the nine elements of the vector dyadic reflectivity function which allows us to determine the orientation and more details of the target. For instance, (Figure 6) represents when both the target and the dipole orientation are along the *x* direction and indeed detection occures, while (Figures 8 and 10) represents dipoles oriented along the y and *z* directions, respectively. The dipole is detected only when both the target and the sensor antenna have the same polarization. Therefore, using the dipole-based model in equation (10) one can determine the orientation of such dipoles, thus providing additional information concerning the target. Note that if a point-scattering model were used, all the nine elements of (Figures 6, 8 and 10) would have appeared equal.

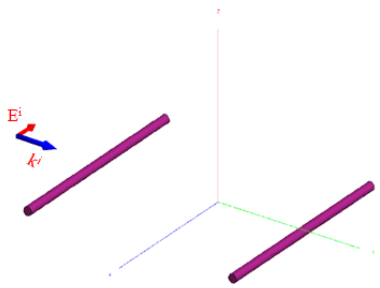

Fig. 5 FEKO model. Two cylinders oriented along x-direction where E^i is the incident plane wave and k^i is the propagation vector.

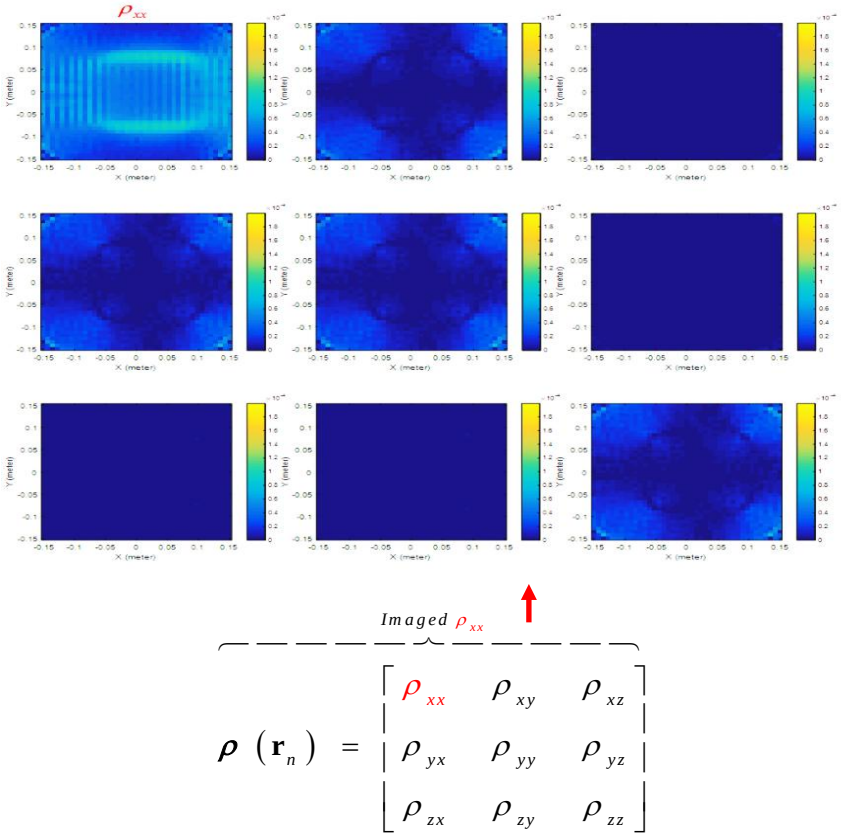

Fig. 6 Simulation result: Two thin cylinders along x-direction are imaged

Figure 6, the target was illuminated from along x-axis and the goal was to image the two cylinders by employing the proposed method known as dipole model (DM) and show that not only we can detect the target and image it but also discren the orientation of the target which is very important. We only got the response of ρ_{xx} out of the nine elements of reflectivity function $\boldsymbol{\rho}(\mathbf{r}_n)$.

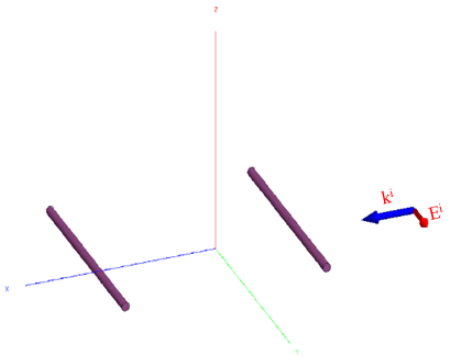

Fig. 7 Two cylinders oriented along y-direction where E^i is the incident plane wave and k^i is the propagation vector.

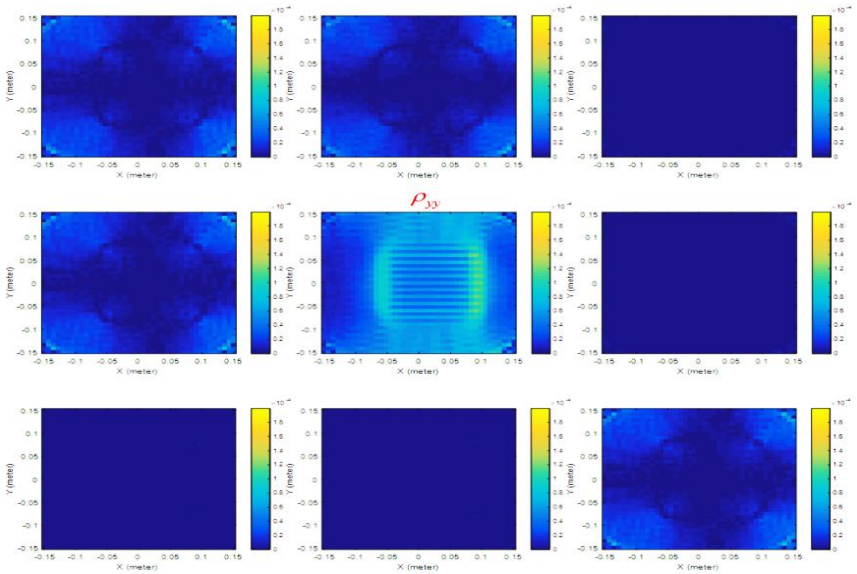

Fig. 8 Simulation result: Two thin cylinders are placed along y-direction

Figure 8, the target and the source (dipole) are placed along y-axis and we got strong response from ρ_{yy} out of the nine elements of reflectivity function $\boldsymbol{\rho}\ (\mathbf{r}_n)$. This shows again that when both the antenna and the target have the same orientation along y-axis ρ_{yy} detection is declared only on a specific location of the reflectivity function and that allows to extract the orientation of the target.

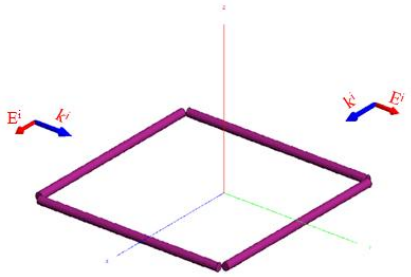

Fig. 9 The geometry of the problem from FEKO. This is four cylinders shaped as a square which is illuminated with incident plane wave E^i both along x - axis and y - axis to create the full image of the four cylinders and k^i is the propagation vector.

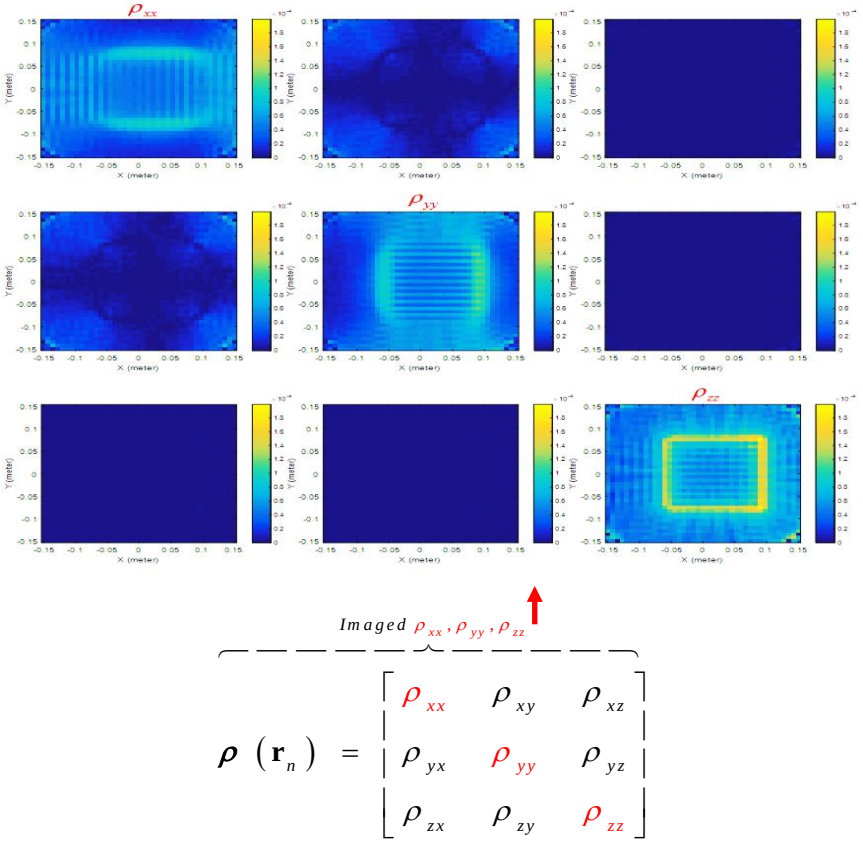

Fig. 10 Simulation result: The reconstructed image of two thin cylinders are placed along x-direction, another two are placed along y-direction which formed square.

Figure 10, is based on reconstructing the full image of (Figure 9) which comprises four cylinders shaped as a square. Finally, we illuminated the target both from x-axis and y-axis as shown in (Figure 9) and we got ρ_{xx}, ρ_{yy} and ρ_{zz} responses as expected and shown in the (Figure 10). This shows that we only get response when the target and the source (dipole) are aligned because when the incident field E^i strikes the target in parallel, a current is induced which in turn creates radiated field. E^s. That radiated field is collected by the receiver (dipole) and detection is declared.

VI. CONCLUSION

In this paper we developed an efficient, practical and improved method for ISAR imaging, known as the dipole model based approach, and we rely upon a vector dyadic reflectivity function which comprises a nine elements rather than point source model. Under the dipole model based approach, we constructed a 2D ISAR

image of two parallel cylinders with different orientation by computing (and plotting) the nine dyadic elements. Each time, detection declaration occurred when the antenna and the cylinders are co-polar, as shown in (see Figures 6, 8 and 10). When the scalar method, which is based upon a point source model, is used, detection occurred each time no matter which angle we illuminated from the target and we were not be able to discren the orientation of the target or have more information about it.

VII. REFERENCES

[1] C. Balanis, Advanced Engineering Electromagnetics, Wiley, 2012.

[2] K. Barkeshli, Advanced Electromagnetics and Scattering Theory, Springer, 2014.

[3] C. OZDEMIR, Inverse Synthetic Aperture Radar Imaging With Matlab Algorithms, Hoboken, New Jersey: John Wiley & Sons INC, 2012.

[4] D. K. Cheng, Field and Wave Electromagnetics, Addison-Wesley Publishing, 1989.

[5] A. Nassib, T. Negishi, D. Erricolo, M. Wicks et L. Lo Monte, «A Dyadic Target Model for Multistatic SAR/ISAR Imaging,» chez *2015 IEEE International Radar Conference*, Arlington, 2015.

[6] A. Nassib, M. Almutiry, Y. Guzel, M. Michael et L. Lo Monte, «FEKO Based ISAR Analysis for 3D Object Reconstruction,» chez *IEEE NAECON Conference* , Dayton, 2015.

[7] M. Gustafsson, «Multi-Static Synthetic Aperture Radar and Inverse Scattering,» LUTEDX/(TEAT-7123)/1-28/(2003), 2004.

[8] J. A. Jackson, Three-Dimensional Feature Models for Synthetic Aperture Radar and Experiments in Feature Extraction, Columbus, OH: PhD Dissertation, The Ohio State University, 2009.

[9] L. Lo Monte, F. Soldovieri, D. Erricolo, A. Giannopoulos et M. C. Wicks, «A Comprehensive Forward Model for Imaging under Irregular Terrain Using RF Tomography,» *nternational Journal of Antennas and Propagation*, vol. Volume 2012, p. 15, 2012.

[10] L. Lo Monte, F. Soldovieri et M. C. Wicks, «Radio Frequency Tomography for Tunnel Detection,» *IEEE TRANSACTIONS ON GEOSCIENCE AND REMOTE SENSING*, vol. VOL. 48, p. NO. 3, MARCH 2010.

[11] R. Harrington, Time-Harmonic Electromagnetic Fields, IEEE Press Series on Electromagnetic. Wiley, 2001.

[12] A. Ishimaru, Electromagnetic Wave Propagation, Radiation and Scattering, Englewood Cliffs: PRENTICE HALL, 1991.

[13] T. Leung, K. Jin et D. Kung, Scattering of ElectromagneticWaves,Theories and Applications, New York: Wiley-Interscience, 2004.

[14] T. A. MILLIGAN, MODERN ANTENNA DESIGN, JOHN WILEY & SONS, INC, 2005.

[15] L. Lo Monte, F. Soldovieri et M. C. Wicks, «RF Tomography for Below-Ground Imaging of Extended Areas and Close-in Sensing,» *IEEE GEOSCIENCE AND REMOTE SENSING LETTERS*, vol. VOL. 7, p. NO. 3, JULY 2010.

[16] M. PASTORINO, Microwave Imaging, WILEY, 2010.

[17] R. L. Moses, L. Potter et M. Cetin, «Wide Angle SAR Imaging,» chez *SPIE Defense and Security Symposium*, 2004.

[18] L. L. MONTE, *Radio Frequency Tomography for Underground Void Detection*, University of Illinois at Chicago, 2009.

[19] J. Nocedal et S. J. Wright, Conjugate gradient methods, Springer, 2006.

[20] Y. Saad, Iterative Methods for Sparse Linear Systems., PWS, 1996.